

RESEARCH ARTICLE

An Artificial Immune System Model Tightly Coupled to the Inverse Design of Photonic Crystals

GILLIARD N. MALHEIROS-SILVEIRA¹, (Senior Member, IEEE),

AND VITALY F. RODRÍGUEZ-ESQUERRE²

¹School of Electrical and Computer Engineering (FEEC), University of Campinas (UNICAMP), Campinas, São Paulo 13083-852, Brazil

²Graduate School of Electrical Engineering, Federal University of Bahia (UFBA), Bahia 40210-630, Brazil

Corresponding author: Vitaly F. Rodríguez-Esquerre (vitaly.esquerre@ufba.br)


This work was supported by the Fundação de Amparo à Pesquisa do Estado de São Paulo (FAPESP) under Project 2015/24517-8, in part by the Bahia State Research Support Foundation (FAPESB) under Grant 079/2016, in part by the Coordination for the Improvement of Higher Education Personnel (CAPES) under Grant 001 and CAPESPrint, in part by the Federal University of Bahia (UFBA), in part by the National Council for Scientific and Technological Development (CNPq) Process 309100/2018-6, and in part by the Fotonicom National Institute of Science and Technology (INCT/CNPQ/FAPESP).

ABSTRACT We propose a model based on an Artificial Immune System (AIS) to be used in conjunction with any electromagnetic solver in order to solve inverse design problems of integrated photonics. The proposed AIS was inspired by the Opt-aiNET algorithm coupled to a homemade electromagnetic solver based on the frequency domain Finite Element Method (FEM), which was used for calculating the fitness function. To validate the proposed model, we evaluate the photonic bandgap (PBG) of photonic crystals by the inverse design approach by assuming triangular lattices comprised of Si and air, and compared the results with other metaheuristics. The proposed AIS model is tightly coupled to such type of problem when the photonic structure is discretized in the binary-valued domain. Interestingly, different from many bio-immune-inspired metaheuristics, this proposed model has one of its metaheuristics parameters highly related to the characteristics of the application, which allows the algorithm itself to get a better “learning” of the problem and, additionally, reveals the designer some features intrinsic to the application. We have obtained midgap ratios of the first PBGs in triangular lattices of 47.55% and 49.11% for transversal magnetic (TM) and transversal electric (TE) polarizations, respectively. Additionally, the proposed model was applied to achieve large PBGs assuming the TM polarization in PhCs based on silicon carbide, and a new structure presented a PBG equals to 33.94%.

INDEX TERMS Artificial immune system, inverse design, photonic crystals, photonic bandgap.

I. INTRODUCTION

Photonic Crystals (PhCs) are periodic arrangements formed by materials with at least two different electric permittivity values, and they can be used to manage/control the flow of light. It can be periodically structured in 1, 2, or 3 dimensions [1], [2]. The PhCs may exhibit photonic bandgap (PBG), which means some or a band of frequencies of light are prohibited from propagating; in other words, the PhCs can operate as a perfect mirror comprised of dielectric materials.

The associate editor coordinating the review of this manuscript and approving it for publication was Santosh Kumar .

This special characteristic of PhCs that inhibits radiation losses may be used to implement several types of optical components like integrated optical waveguides, optical fibers, filters, couplers, power splitters, all-optical logical gates, and adders, among others [2], [3], [4]. Therefore, the demand for bandwidth in modern optical communication systems for the transmission and for processing of data in the optical domain requires the use of wideband optical devices such as couplers, waveguides, and modulators. The design of compact devices for large wideband operations needs the use PhCs exhibiting large PBGs. The inverse design of PBG materials can be conducted by exploring the PhC parameters like lattice

type, symmetry reduction, refractive indexes, filling factor (fraction), and shape. The above-mentioned geometric and material parameters result in a vast combinational problem, which requires algorithms capable of exploring the search space with reduced time and/or computational effort. On the other hand, techniques like neural networks can also be used to calculate band diagrams and PBGs [5], [6] with good precision and reduced computational time, as well as optimize PhC nanocavities [7], [8]. Several publications related to the optimization of photonic devices have been published lately. Additionally, as shown in [9] and [10], recent results demonstrated the usefulness of inverse design for discovering novel photonic devices for novel applications in situations where the traditional intuition-based procedures fail.

In this study, we considered PhCs, defined in the binary-valued domain, with triangular lattices composed of silicon and air in order to compare the output of our model with the literature [11]. Among the several well-known computational methods to obtain the propagation properties of photonic crystals, such as the Plane Wave Expansion (PWE) [12], Frequency Domain Finite Difference (FDFD) [13], and Frequency domain Finite Element Method [14], we opted for using the latter for its advantages over the formers to analyze nonregular geometries with a moderate computational cost. A homemade electromagnetic solver with a formulation based on the frequency-domain finite element method (FEM) [15] was applied to compute the band diagrams, from where the PBGs' magnitude values are extracted. Such a parameter is used to feed the fitness function of the meta-heuristics used in this study.

In previous works, bio-inspired metaheuristics like a genetic algorithm (GA) and evolutionary algorithms [15], [16], [17], swarm intelligence (SI) algorithms like artificial bee colony (ABC) [11], [18] were used in the binary domain to optimize PBG via inverse design. To the best of our knowledge, immune-inspired metaheuristics [19], [20] have been explored neither in the binary domain nor in problems related to the inverse design of integrated photonics in a way that truly explores their potential. These metaheuristics have some intrinsic and exciting features, reviewed in the methods section, that may be explored to solve the inverse design of photonic structures, and this is the primary motivation to perform this study.

We selected the opt-aiNET [20] as a reference of AIS, and proposed a model based on it, which is dedicated to solving problems defined in the binary domain, which we named Bopt-aiNET. Some main features of the opt-aiNET that excels or are not present in those algorithms, in our point of view, are dynamically adjustable population size, exploration and exploitation of the search space, and location of multiple optima. For example, those could bring a better exploration and exploitation of the search space. Because of that, this could be an excellent opportunity to study its potential applied to this type of problem. Especially when assuming a binary version of the opt-aiNET algorithm, it can provide a final component design more suitable for fabrication

tolerances since the discrete domain may obey such constraints. The novelty of the present work is the implementation of the binary counterpart of the continuous Ainet [20] with all its advantages and the use of the filling factor as the affinity, which takes into account the physics of the problem, giving insights about the needed properties of the photonic crystal to maximize its photonic band gap.

In the next session, there are some brief reviews regarding PhCs/PBG, FEM in the frequency domain, and the opt-aiNET algorithm before introducing our proposal: the Bopt-aiNET one. In section III (numerical results and discussions), we assess the algorithm characteristics for a class of photonic structure, for such case the model is used to maximize the PBG of two different structures, one operating in transversal magnetic (TM) polarization modes and the other in transversal electric (TE) polarization modes. These results are compared to the literature. Additionally, a case study is performed in order to achieve large PBG in PhCs based on silicon carbide. In section IV, we compile the main conclusions of this study.

II. MATERIALS AND METHODS

In this section, we perform a brief review of the PhCs/PBG, FEM in the frequency domain, opt-aiNET algorithm, and introduce the Bopt-aiNET.

A. APPLICATION: PHOTONIC CRYSTALS AND PHOTONIC BANDGAP ENGINEERING

Photonic crystals are inhomogeneous materials with periodic structures in one-, two-, or tri-dimensions, where the dielectric properties vary periodically along the periodic directions on the order of the light wavelength. The PhCs are governed by the Bloch-Floquet theorem [21] and have their behavior described by Maxwell's equations. Basically, PhCs comprised of dielectric materials interact with photons in a similar way as semiconductor crystals deal with electrons [1], [2], e.g., in analogy to a semiconductor crystal that has a forbidden gap, PhCs may present photonic bandgap (PBG). The former means that photons with frequency or energy into the PBG are not allowed to propagate through the PhC. This exceptional property of PhCs, e.g., can be used to implement dielectric mirrors of high reflectivity. In integrated photonics, PhCs are considered as building blocks to realize components, where the operating principle relies basically on the PBG and not on the total internal reflection, which is derived from Snell's law.

In this work, we arbitrarily choose to deal with the inverse design of 2-D PhCs with large PBGs in order to assess the Bopt-aiNET algorithm. In summary, 2-D PhCs are periodic in two dimensions and homogeneous in the third one (see Fig. 1.a). Also, they may be commonly produced by: fabricating periodic pillars embedded in a low refractive index substrate or drilling a periodic array of holes in a dielectric slab. Although the pillars or holes geometry are generally cylinders, their geometry may be arbitrary. Figure 1.a shows the schematics of a 2-D PhC comprised of periodic pillars,

arranged in a square lattice, of silicon embedded in air. The correspondent first Brillouin zone and band diagram for PhC comprised of pillars with radii assuming $r = 0.2a$ are shown in Fig. 1.b and Fig. 1.c, respectively, where PBG for the TM modes are highlighted, a is the constant lattice or periodicity.

The dispersion diagram presented in Figure 1.c relates the propagation direction of the wave (TE and TM polarized modes in red and blue curves, respectively) and its phase velocity represented by the wavevector, composed of two components k_x and k_y (horizontal axis) as a function of the operating frequency (vertical axis). It can be observed that some frequency bands do not possess an associated wavevector; consequently, those frequencies can not propagate in the photonic crystalline structure.

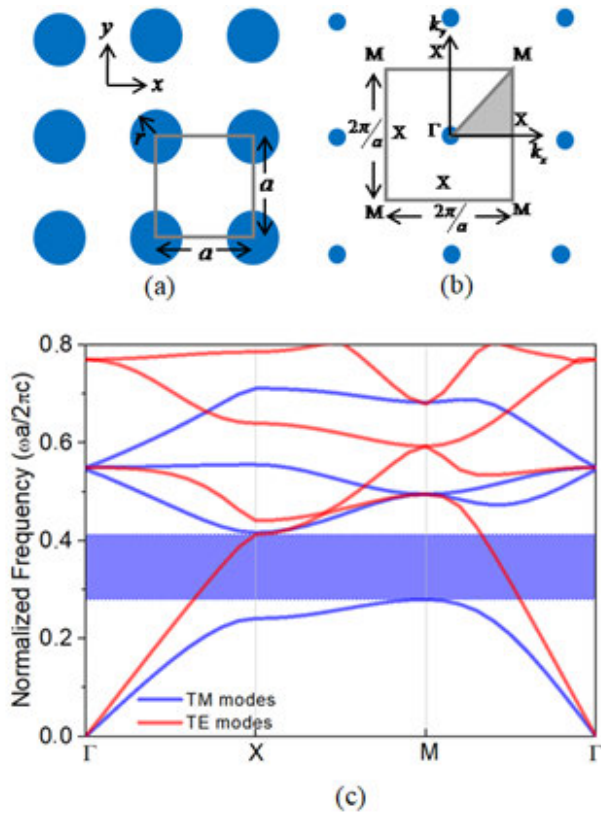


FIGURE 1. (a) PhC structured in cylindrical pillars of silicon in a square lattice, and related (b) first Brillouin zone, and (c) band diagram for $r = 0.2a$, highlighting the PBG for TM modes.

It can be noticed that a 2-D PhCs structured as that represented in Fig. 1.a may produce PBGs for TM polarization mode. On the other hand, periodic holes in dielectric slabs are more suitable to present PBG for the TE polarization mode. It is also known from the literature [2], [7] that 2-D PhCs in triangular lattices tend to produce larger PBGs than in square lattices. All this information present in this paragraph will be considered as heuristics for our inverse design approach.

B. NUMERICAL SOLVER: FINITE ELEMENT METHOD FOR PHC ANALYSIS

The two-dimensional triangular lattice is shown in Fig. 2, for the sake of simplicity, it is represented by circular elements inside the unitary cell.

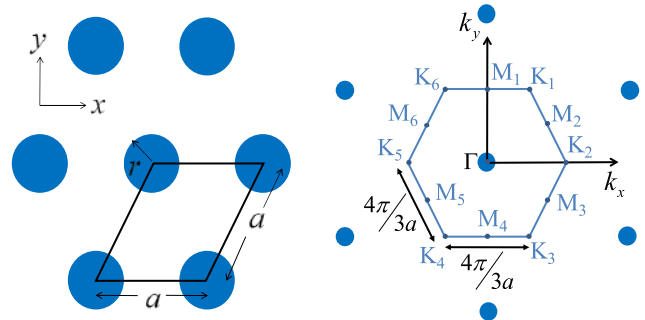


FIGURE 2. Two-dimensional triangular lattice (left) and correspondent first Brillouin zone (right).

For PBG calculation, we just need to analyze the unitary cell imposing appropriated boundary conditions by using the frequency domain 2D FEM approach [8], [15]. The FEM analysis of 2D PhCs can be applied separately for each polarization mode (TE and TM). In any case, we start from the second-order wave equation given by,

$$-\frac{\partial}{\partial x} \left(p \frac{\partial \Phi}{\partial x} \right) - \frac{\partial}{\partial y} \left(p \frac{\partial \Phi}{\partial y} \right) = q \left(\frac{\omega}{c} \right)^2 \Phi \quad (1)$$

where, $p = 1/n$, $q = 1$ and $\Phi = E_z$ for the TE modes, and $p = 1$, $q = n$ and $\Phi = H_z$ for the TM modes. Here, n is the refractive index of either air ($n = 1.0$), silicon ($n = 3.478$) or silicon carbide ($n = 2.6$). The fields E_z and H_z can be written as

$$E_z = e_z e^{-jk_x x} e^{-jk_y y} \quad (2)$$

$$H_z = h_z e^{-jk_x x} e^{-jk_y y} \quad (3)$$

where, e_z and h_z are the fields' spatial envelopes and k_x and k_y are the propagation constants in the x and y direction, respectively, whose values are restricted to the first Brillouin zone [2], see Fig. 2. Substituting (2) in (1), applying the conventional Galerkin method [15] and discretizing the computational domain using 6-node isoparametric second-order triangular elements we obtain an eigenvalue problem given by,

$$[A] \{\phi\} = \left(\frac{\omega}{c} \right)^2 [B] \{\phi\} \quad (4)$$

where the vector $\{\phi\}$ is the e_z or the h_z field. For TE modes, matrices $[A]$ and $[B]$ are given by,

$$[A] = \sum_e \left[\iint_e \frac{1}{n_o^2} \frac{\partial \{N\}}{\partial x} \frac{\partial \{N\}^T}{\partial x} dx dy + \iint_e \frac{1}{n_o^2} \frac{\partial \{N\}}{\partial y} \frac{\partial \{N\}^T}{\partial y} dx dy \right]$$

$$\begin{aligned}
& + jk_x \iint_e \frac{1}{n_o^2} \left(\frac{\partial \{N\}}{\partial x} \{N\}^T - \{N\} \frac{\partial \{N\}^T}{\partial x} \right) \partial x \partial y \\
& + jk_x \iint_e \frac{1}{n_o^2} \left(\frac{\partial \{N\}}{\partial y} \{N\}^T - \{N\} \frac{\partial \{N\}^T}{\partial y} \right) \partial x \partial y \\
& + \iint_e \frac{1}{n_o^2} \left(k_x^2 + k_y^2 \right) \{N\} \{N\}^T \partial x \partial y \Big] \quad (5)
\end{aligned}$$

$$B = \sum_e \iint_e \{N\} \{N\}^T \partial x \partial y \quad (6)$$

For TM modes, matrices [A] and [B] are given by,

$$\begin{aligned}
[A] = \sum_e \Bigg[& \iint_e \frac{\partial \{N\}}{\partial x} \frac{\partial \{N\}^T}{\partial x} \partial x \partial y \\
& + \iint_e \frac{\partial \{N\}}{\partial y} \frac{\partial \{N\}^T}{\partial y} \partial x \partial y \\
& + 2jk_x \iint_e \frac{\partial \{N\}}{\partial x} \{N\}^T \partial x \partial y \\
& + 2jk_x \iint_e \frac{\partial \{N\}}{\partial y} \{N\}^T \partial x \partial y \\
& + \iint_e \left(k_x^2 + k_y^2 \right) \{N\} \{N\}^T \partial x \partial y \Big] \quad (7)
\end{aligned}$$

$$B = \sum_e \iint_e n_e^2 \{N\} \{N\}^T \partial x \partial y \quad (8)$$

$\{N\}$ are the elementary matrices from the FEM formulation, and T denotes the transpose [14]. Since the PhC is, ideally, a periodic structure, we just need to discretize one unitary cell. Then, periodic boundary conditions are applied by making equal the fields at the left and right sides and the fields at the top and bottom of the unitary cell. In our simulations, we are dealing with lossless dielectrics; consequently, losses are not present. However, in practical an application, we can observe radiation losses since the structure has a finite length in the z direction, and power could be radiated to the free space.

C. OPT-AINET

The opt-aiNET algorithm is an immune-inspired algorithm for function optimization [20], where the population is comprised of a network of antibodies (candidate solutions). Basically, the algorithm consists on the evaluation of the objective function, clonal expansion, mutation, and selection. The algorithm also creates a memory of antibodies comprised of the best candidate solutions to the objective function and is capable of optimizing either unimodal or multimodal functions. The main features are dynamically adjustable population size; exploration and exploitation of the search space; location of multiple optima; capability of maintaining many optima solutions; and defined stopping criteria.

For clarity's sake, we briefly review the terminology and algorithm of the opt-aiNet [20] (proposed for real-valued domain) as follow:

- Network cell: individual of the population. In this case, no encoding is performed; each cell is a real-valued vector in a Euclidean shape-space;
- Fitness: fitness of a cell in relation to an objective function to be optimized. The value of the function when evaluated for the given cell;
- Affinity: Euclidean distance between two cells;
- Clone: offspring cells that are identical copies of their parent cell.

The algorithm proposed by [20]:

1. Randomly initialize a population of cells
2. While the stopping criterion is not met do
 - 2.1 Determine the fitness of each network cell and normalize the vector of fitnesses.
 - 2.2 Generate a number N_c of clones for each network cell.
 - 2.3 Mutate each clone proportionally to the fitness of its parent cell, but keep the parent cell. The affinity proportional mutation uses the eq. 1 in [20].
 - 2.4 Determine the fitness of all individuals in the population.
 - 2.5 For each clone, select the cell with the highest fitness and calculate the average fitness of the selected population.
 - 2.6 If the average error of the population is not significantly different from the previous iteration, then continue. Else, return to step 2.1
 - 2.7 Determine the affinity of all cells in the network. Suppress all but the highest fitness of those cells whose affinities are less than the suppression threshold σ_s and determine the number of network cells, named memory cells, after suppression.
 - 2.8 Introduce a percentage $d\%$ of randomly generated cells and return to step 2.
3. EndWhile

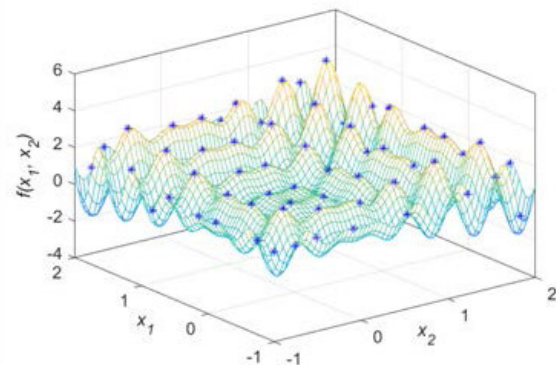


FIGURE 3. Search space defined by the Multi function (1), and the optimal solutions obtained by opt-aiNET for a real-valued domain.

Figure 3 shows the assessment of our implementation of the opt-aiNET proposed by [20] applied to the Multi function (a real-valuated one), described by the following equation:

$$f(x_1, x_2) = x_1 \sin(4\pi x_1) - x_2 \sin(4\pi x_2 + \pi) + 1 \quad (9)$$

where x_1 and $x_2 \in [-1, 2]$.

From this assessment, we verified the main features of the opt-aiNET previously mentioned, which motivated us to adapt this algorithm to the inverse design of integrated photonic structures.

D. PROPOSED MODEL: BOPT-aiNET

In this section, we introduce the Bopt-aiNET (Binary Opt-aiNET) algorithm. This model aims to provide an AIS approach tightly coupled to a binary search space in order to solve computational electromagnetic problems using the inverse design approach.

The dynamics of this algorithm, as it should be, are similar to the opt-aiNET one. However, the main differences are:

- The search space or individual representation is defined by a binary-valued vector;
- The affinity is neither defined by a Euclidian distance, as done in real-valued domain, nor by Hamming distance, as in [23]; actually, it is defined by the filling fraction of the network cells, and the benefits of this are going to be highlighted in the next section.
- The mutation is not defined by a specific function, although it has a higher rate for network cells with lower fitnesses;
- In general, as expected, the operations are performed in a binary domain.

The class of problem chosen to evaluate the proposed model requires the numerical solution of Maxwell’s equations. For this purpose, we choose the FEM; which requires the discretization of the problem domain in a mesh composed of triangles. Thus, the search space is a discrete one. Also, because each cell of the mentioned mesh may be occupied by one type of material (between two options) in order to compose the unitary cell of the PhC, the search space becomes binary.

Figure 4 shows the schematic of binary codification for PhCs structured in a triangular lattice, and discretized in a coarse mesh of 6×6 triangles for the sake of clarity.

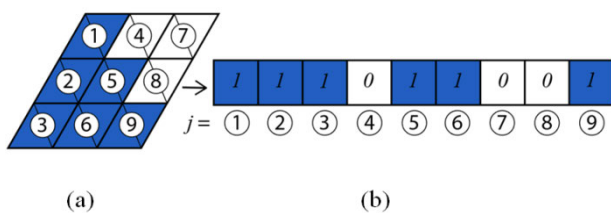


FIGURE 4. Example of binary codification of the network cell (a) PhC’s unit cell discretized in a coarse mesh of 18 triangular elements. (b) Binary representation for the PhC’s unit cell with 9 optimization parameters.

Each pair of triangles is labeled by the index j , and represents the minimal portion of the unitary cell of the PhC; whose values are binary numbers defined by the algorithm. In other words, in this example, the binary codification produces a network cell with 3×3 variables or portions. Arbitrary, “0’s” represent lower refractive index material (air), and “1’s” represents the higher refractive index one (silicon). We assumed the refractive index of Si as $n = 3.478$ [24] and $n = 1$ for air. In order to assess the proposed algorithm, the simulations were performed in a 10×10 binary domain, which represents a search space of 2^{100} PhC configurations.

In the following, we introduce the adaptations we made in the algorithm taken as reference, Opt-aiNET [20] (which was proposed for the optimization of problems in a real-valued domain), in order to perform the inverse design of PhCs structures defined in a binary domain:

Initial Population: All network cells (individuals) of the first generation are randomly created. As reported in the literature, if the PhC is comprised only of two materials (e.g., Silicon and air), commonly, the PhC will present PBG when its geometry is comprised of materials arranged in clusters [14], [15]. Figure 5.a, shows an example of a unit cell with its structure formed by a dispersed portion of material. This type of configuration, although it may allow PBG formation, has more constraints during the fabrication processes. Some proposal for optimization model does not need to take this issue into account [23].

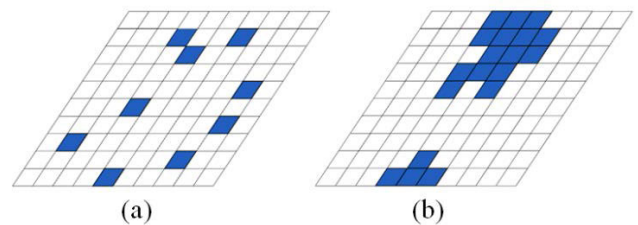


FIGURE 5. Examples of unitary cells representing (a) dispersed portions of silicon (generally, undesired due to fabrication complexity) and (b) clusters of silicon.

Figure 5.b shows material clusters (this one generally allows PBG formation and has fewer constraints during the fabrication processes). A hint is incorporated in the code in order to produce potential and feasible solutions right at the first generation.

Mutation: This operator mutates a number of bits in each clone inversely proportional to the fitness of the parent cell. Basically, the parent cells are ordered in descending order according to their fitness value, and the position that each parent cell occupies corresponds to the number of bits to be mutated in their respective clones.

Fitness: The fitness function is obtained from the PBG calculation for one type of mode polarization, TE or TM mode, of the PC. The PBGs for the TE_{1-2} or TM_{1-2} polarization

modes are quantified by the gap-to-midgap ratio:

$$f = \frac{E_{top} - E_{bottom}}{E_{middle}} \times 100\% \quad (10)$$

where E_{top} , E_{bottom} , and E_{middle} mean the lower frequency of the higher mode, the upper frequency of the lower mode, and the average of these two previous frequencies, respectively. For the sake of clarity, the position of these frequencies is represented in the sketch depicted in Fig. 6, assuming a PhC with a square lattice.

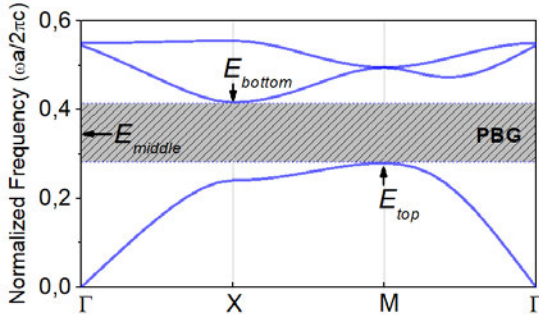


FIGURE 6. Schematic of the band diagram example highlighting the positions of the E_{top} , E_{bottom} and E_{middle} .

To calculate PBG for unit cells with asymmetric structures, we need to solve the problem at the labeled points in the first Brillouin zone shown in Fig. 2. If we assume that the problem has folded symmetry, they can be limited by $M(0,2\sqrt{3}/3)\pi/a - \Gamma(0,0)\pi/a - K(2/3,2\sqrt{3}/3)\pi/a - M(0,2\sqrt{3}/3)\pi/a$ for triangular lattices (see Fig. 2). In the inverse design problem treated in this study, the inner configuration of the unitary cell (spatial material disposition) was considered to present the most arbitrary geometry. Thus, we need to solve all the labeled points because minimum and maximum frequencies lie in those points. Consequently, we have to compute the PBG at thirteen points (Γ , M_1 , K_1 , M_2 , K_2 , M_3 , K_3 , M_4 , K_4 , M_5 , K_5 , M_6 , K_6) [16] when assuming triangular lattices. The computational cost and processing time are considerably reduced by considering such points instead of the entire Brillouin zone. Additionally, we arbitrarily look for PBG between the TE_{1-2} or TM_{1-2} modes.

The affinity is determined by the filling fraction of the network cells. The algorithm will suppress the network cells with the same value of filling fraction and having the lowest fitness (in other words, the suppression threshold, σ_s , equals zero according to our affinity definition).

III. NUMERICAL RESULTS AND DISCUSSION

A. ALGORITHM ASSESSMENT

The parameters used for the Bopt-aiNET are listed in table 1.

The fitness evaluations of structures for the TM and TE polarization modes as a function of generations are shown in Fig. 7. The number of memory cells per generation is not fixed (the population size is dynamic); this is one of the algorithm characteristics. A large diversity of individuals,

TABLE 1. BOPT-AINET's control parameters for the maximization.

Bopt-aiNET Parameters	Values
Initial population size	4
Number of clones	4
Number of randomly generated cells	2
Maximum number of generations	600

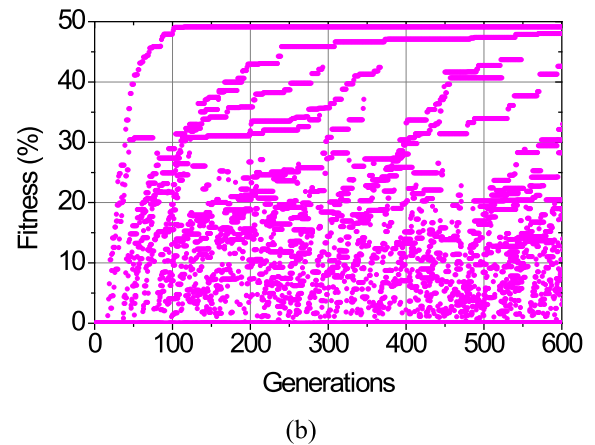
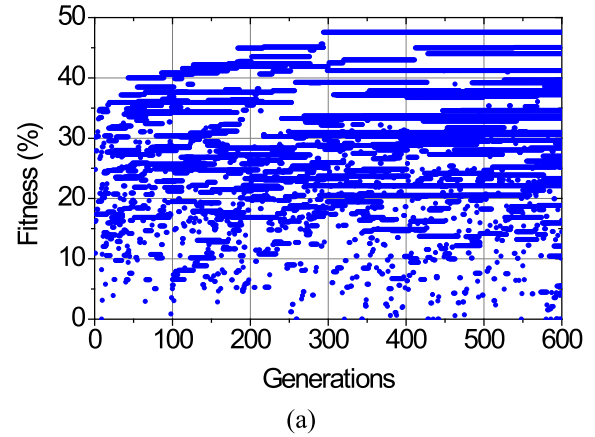
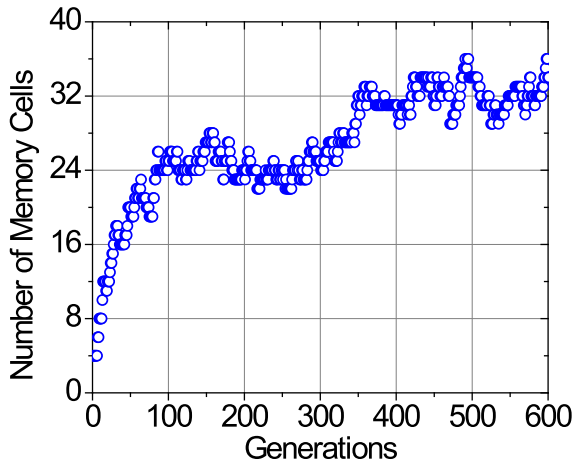


FIGURE 7. Fitness of the structures versus generations for the (a) TM_{1-2} (b) TE_{1-2} polarizations.

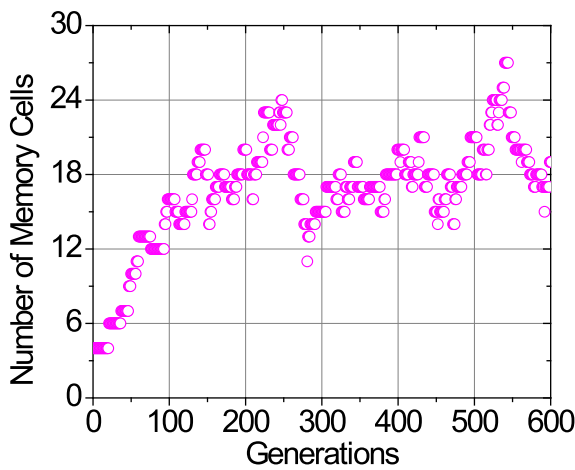
demonstrated by the diversity of fitness, is also observed, meaning the algorithm performed a good sweep of global search. Additionally, many memory cells exhibit a good fitness value. It can be attributed to the coarse mesh discretization of the unitary cell of the PhC.

Figure 8 makes evident the number of memory cells per generation. Although the initial population started with 4 (four) network cells, the final generation ended up with a larger amount of memory cells. These curves also reveal another interesting characteristic of the algorithm, which is the size control of the memory cells, avoiding a quick growing of the memory cells' size.

The filling fraction of the memory cells per generation is shown in Fig. 9. Although different network cells may present the same filling fraction value, this figure makes



(a)



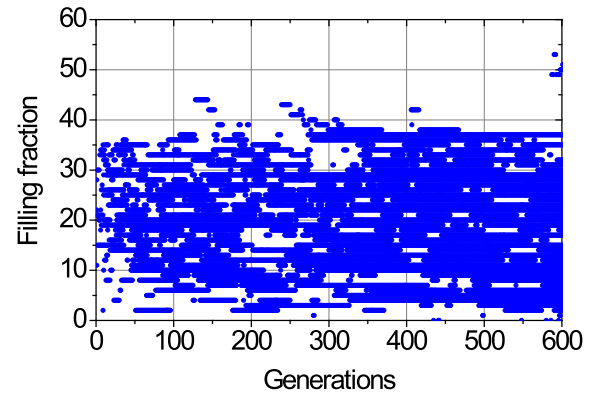
(b)

FIGURE 8. The number of memory cells per generation for the (a) TM_{1-2} (b) TE_{1-2} polarizations.

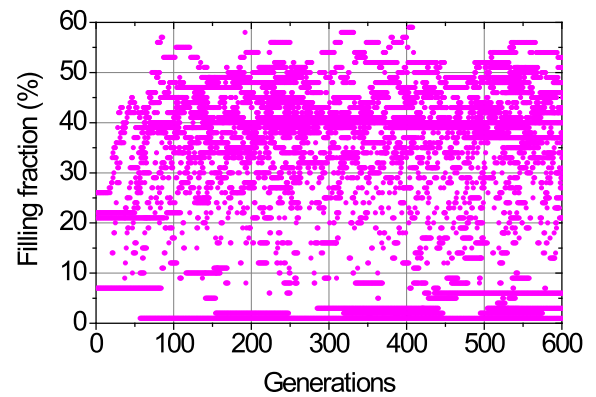
evident the algorithm explored a large sweep of network cell configurations.

Figure 10.a shows the fitness versus the filling fraction for the TM_{1-2} mode. This graph reveals the cells with the highest fitness have about 10% filling fraction, also some cells with a filling fraction above 55% were suppressed by the affinity defined in our approach. On the other hand, Fig. 10.b shows a similar relation for the TE_{1-2} mode. For this graph one can see the cells with the highest fitness have about 40% filling fraction; also some cells with a filling fraction above 60% were suppressed by the affinity. Because of the stochastic nature of this class of algorithm, not necessarily cells with all possible filling fractions were produced during the algorithm run. Furthermore, this type of output can be used as a start condition in another run, with refined mesh, by delimiting the search space to PhC configurations with filling fractions nearby those ones of higher fitness values.

Another interesting characteristic is represented in Fig 11. In the figure, it is shown the number of suppressed network cells versus the generation that suppression occurs. First, it is



(a)



(b)

FIGURE 9. Filling fraction of memory cells per generation for the (a) TM_{1-2} (b) TE_{1-2} polarizations.

noticed that suppression only occurs in some generations. Second, when suppression takes place, a variable number of network cells are suppressed from that population.

A schematic of the optimized structure for the TM_{1-2} polarization obtained by the Bopt-aiNET is shown in Fig. 12, and the configuration of the unit cell obtained for the triangular arrangement on a 10×10 -sized domain is shown as an inset. Although the unity cell geometry is not intuitive, it is defined by high-index material columns embedded in low-index material, which is a type of structure expected from the theory for large PBG in TM polarization [2]. The band diagram for this PhC is shown in Fig. 13 where the PBG is highlighted.

A schematic of the optimized structure for the TE_{1-2} is shown in Fig. 14, and the configuration of the unit cell obtained for the triangular arrangement on a 10×10 -sized domain is shown as an inset. For this case, the unity cell geometry also is not intuitive, and it is defined by connected high-index material lattices embedded in low-index material, which is a type of structure expected from the theory for maximum PBG in TE polarization [2]. The band diagram for this PhC is shown Fig. 15, where the PBG is also highlighted.

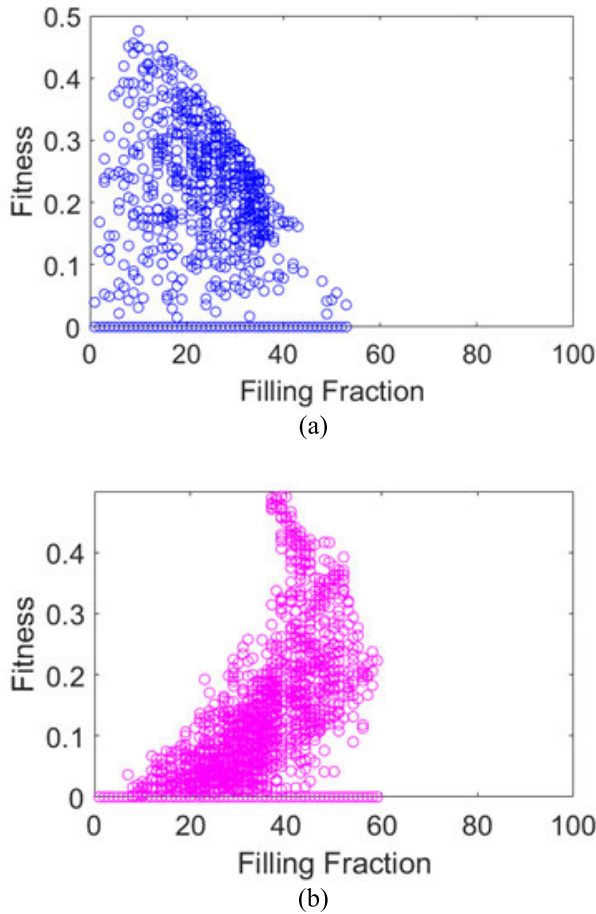


FIGURE 10. Fitness versus Filling fraction for the (a) TM_{1-2} (b) TE_{1-2} polarizations.

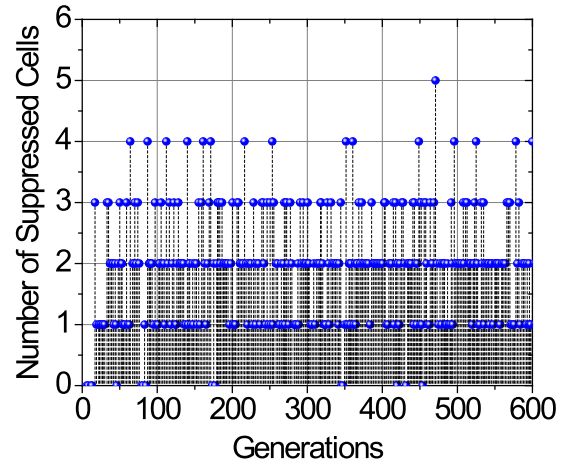
TABLE 2. Results from the BOPT-AINET, ABC, and GA for the PBG optimization in triangular lattices.

Polarization	PBG* by GA [14]	PBG* by ABC [15]	PBG* by Bopt-aiNET
TM_{12}	~ 42.01%	~ 47.55%	~ 47.55%
TE_{12}	~ 48.94%	~ 49.11%	~ 49.11%

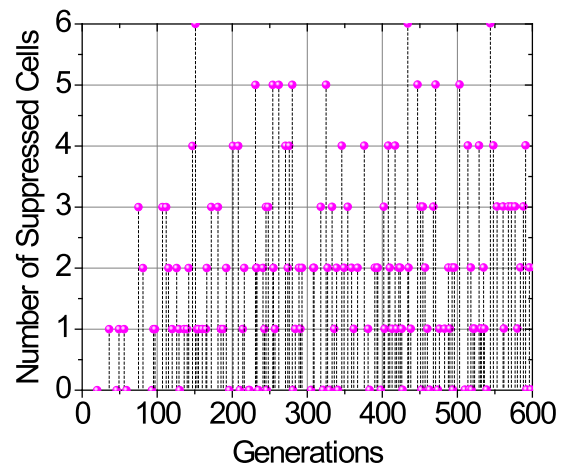
*It refers to the gap to the mid-gap ratio, eq. (9).

In general, if a mesh of higher resolution is used, it probably may allow the algorithm to reach higher PBG values. However, because of the fabrication constraints for such dimensions assuming the current fabrication technology as well as for the sake of assessing the results reached from the proposed model, we decided to keep in this study the mesh resolution of 10×10 .

In this work, we treat PBGs in lower order modes (TE_{1-2} and TM_{1-2}) for comparison purposes, and Table 2 summarizes the results of this study and compares them with related works in the literature. The results obtained from Bopt-aiNET reached the maximum values obtained by the ABC algorithm, both for TE and TM polarizations.



(a)



(b)

FIGURE 11. The number of suppressed cells versus generation of occurrence for the (a) TM_{1-2} (b) TE_{1-2} polarizations.

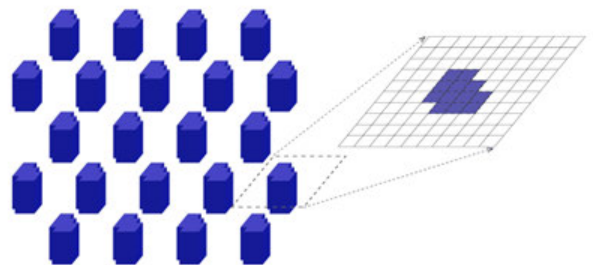


FIGURE 12. Scheme of the PhC corresponding to the TM_{12} polarization optimized for maximum PBG. Inset highlight the respective discretized unit cell.

One may notice from the presented results that the main features of the original opt-aiNET algorithm remain in this novel model: dynamically adjustable population size; exploration and exploitation of the search space; location of multiple optima; capability of maintaining many optima solutions; and defined stopping criteria.

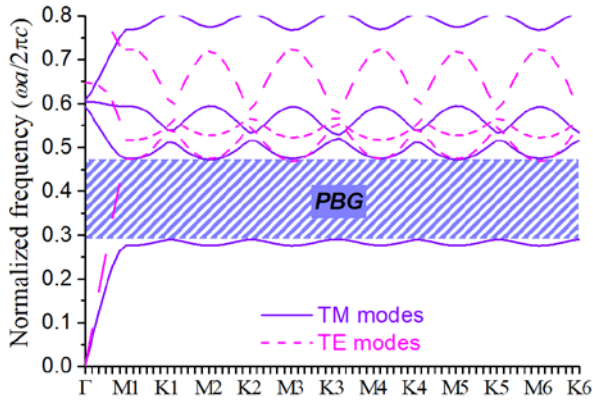


FIGURE 13. Band diagram of the PhC corresponding to the TM₁₋₂ modes optimized for maximum PBG (TM modes are represented in solid lines and TE modes in dashed ones). The correspondence between the x-axis and the key points at the edges/corners of the first Brillouin zone is found in Fig 2.

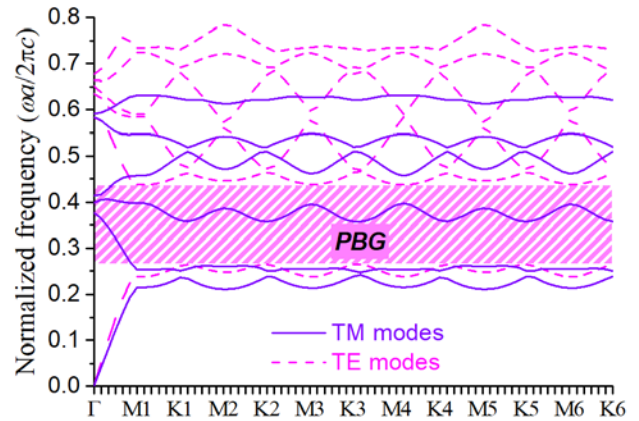


FIGURE 15. Band diagram of the PhC corresponding to the TE₁₂ modes optimized for maximum PBG (TM modes are represented in solid lines and TE modes in dashed ones). The correspondence between the x-axis and the key points at the edges/corners of the first Brillouin zone is found in Fig 2.

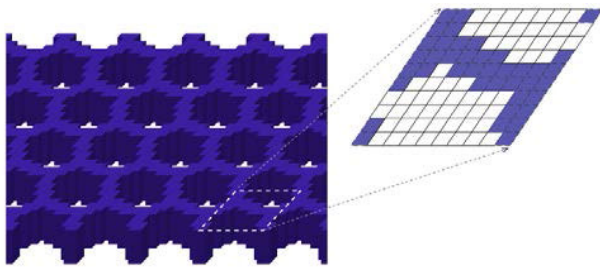


FIGURE 14. Scheme of the PhC corresponding to the TE₁₋₂ polarization optimized for maximum PBG. Inset highlights the respective discretized unit cell.

Interesting noticing that the Bopt-aiNET has some remarkable characteristics in its composition, which in our opinion, brings advantages compared to GA and ABC. The main one is the definition of affinity, which was described as the filling fraction of high-index material related to low-index material. In this case, the representation between the fitness versus filling fraction, as represented in Fig. 10, brings an insight into the Physics of the problem regarding the optimal crystal configurations.

It is difficult to perform a fair comparison between the proposed algorithm and other ones based on distinct meta-heuristics/paradigms like GA (evolutionary algorithm) and ABC (swarm intelligence). This is especially difficult when those meta-heuristics are applied to a very time-consuming category of problem, and it is out of the purpose of this manuscript. Therefore, the accuracy and computational time of the present work is in the same order as the two other methods used for assessment, GA and ABC.

Although the proposed strategy has been applied to the optimization of PBGs in isotropic materials, the same can also be applied to problems considering absolute/complete PBGs [15], [25], [26]. Recent applications require the use of independent polarization mode operation photonic devices, and in that case the PBG for TE and TM modes should

be optimized simultaneously. For this purpose, it may be necessary the use anisotropic materials [26]. In general lines, different types of integrated photonic components [27, 28, 29, 30] can also be designed by the proposed model.

B. INVERSE DESIGN OF PHC BASED ON SILICON CARBIDE (SiC) AND AIR WITH LARGE PBG FOR TM₁₋₂ POLARIZATION

Once the assessment of the capabilities of our proposal was performed by comparing them with results already reported in the literature, in this section, we will apply the same parameters used in the previous section, however assuming an integrated platform based on SiC and air.

SiC offers a broad range of interesting properties, such as a high-refractive index, wide bandgap, high optical nonlinearities, and controllable artificial spin defects, among others. Those properties enabled a myriad of nano-photonic opportunities, such as micro-cavities, waveguides, nonlinear frequency converters, and optically-active spin defects [31]. Additionally, SiC PhCs cavities with high-quality factors and low volume are a promising platform for high-performance nonlinear photonic applications, such as wavelength conversion, harmonic generation, and all-optical switching [32].

In this case study, we assumed the refractive index of SiC as $n = 2.6$ [32], and the algorithm parameters shown in table 1 were kept. The fitness, number of memory cells, and filling fraction of the memory cells, all of them versus generations, are shown in Figures 16, 17, and 18, respectively. Also, the fitness versus filling fraction and number of suppressed cells versus generation of occurrence are shown in Figures 19 and 20, respectively.

The curves shown in Figures 16, 17, 18, 19, and 20 demonstrate the algorithm’s performance in solving this case study. We can notice that, in general, all of them present a pattern that is more similar to the case study related to the optimization of PBGs of PhC composed of silicon/air, for

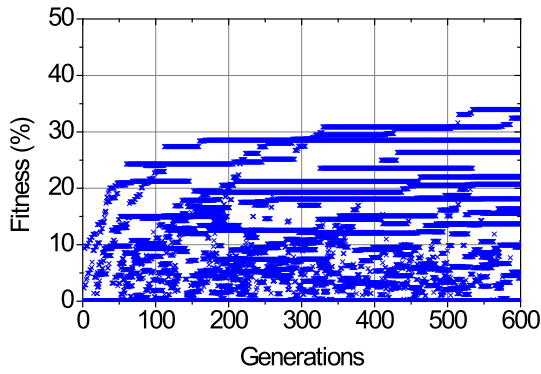


FIGURE 16. Fitness of the structures versus generations for the TM_{1-2} polarizations.

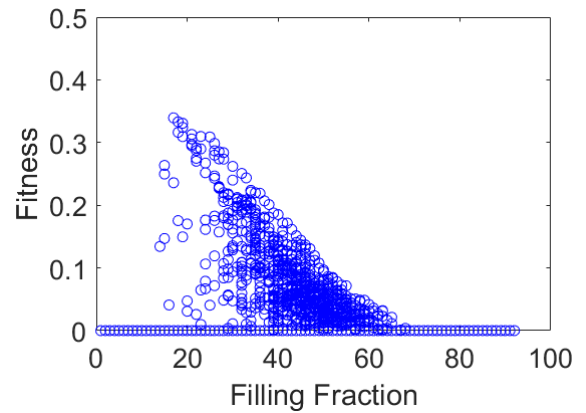


FIGURE 19. Fitness versus Filling fraction for the TM_{1-2} polarizations.

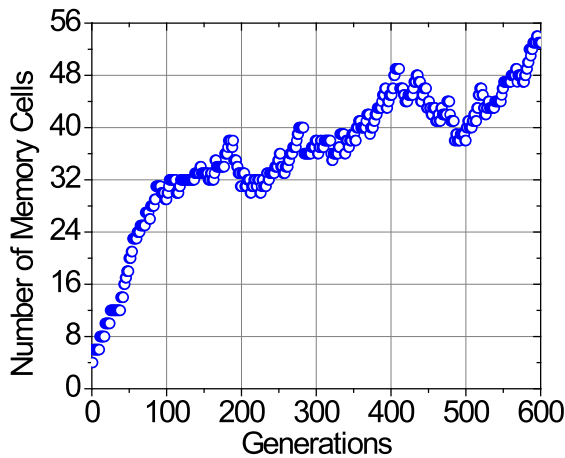


FIGURE 17. The number of memory cells per generation for the TM_{1-2} polarizations.

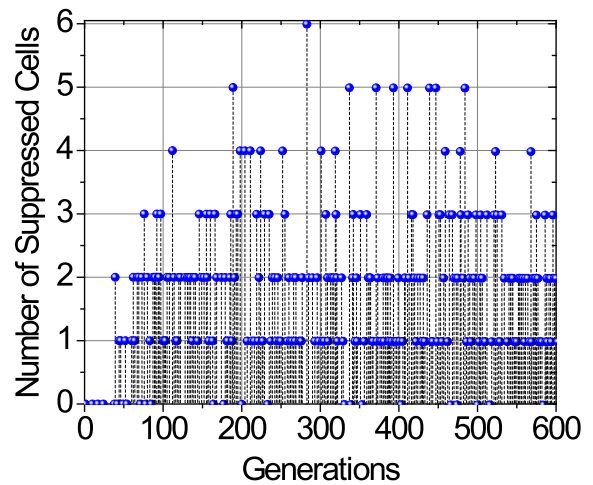


FIGURE 20. The number of suppressed cells versus generation of occurrence for the TM_{1-2} polarizations.

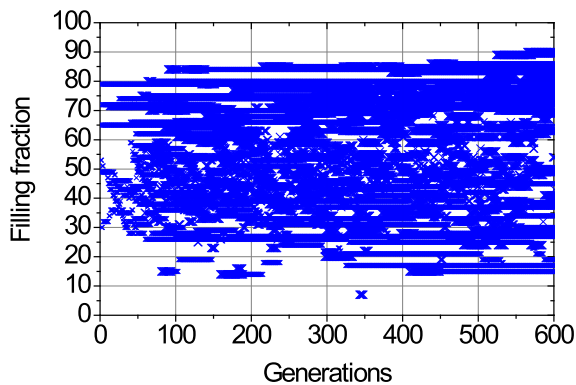


FIGURE 18. Filling fraction of memory cells per generation for the TM_{1-2} .

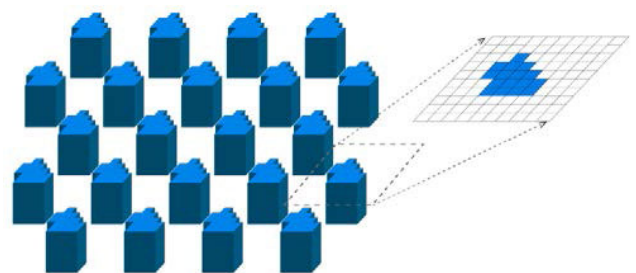


FIGURE 21. Schematic of the PhC corresponding to the TM_{12} polarization optimized to maximum PBG. Inset highlights the respective discretized unit cell.

TM polarizations, than in the case of TE polarizations. These characteristics of the algorithm were discussed in the previous section (3.1) during the algorithm assessment.

A schematics novel structure optimized for the PhC with maximized PBG for the TM_{1-2} polarization, and comprised of SiC and air, is shown in Fig. 21. It can be noticed that the optimal geometry reached by the algorithm is comprised of a cluster/island of SiC embedded in air, without small isolated

pixels/elements; which is useful for further fabrication of such a structure. Its band diagram is shown in Fig. 22, where the PBG for the TM polarization is highlighted, assuming the value of 33.94%. Even though the fitness function did not consider simultaneous PBG optimization for both polarization (TM and TE), the final structure optimized for TM polarization also presents a PBG in TE polarization, as highlighted in that same figure.

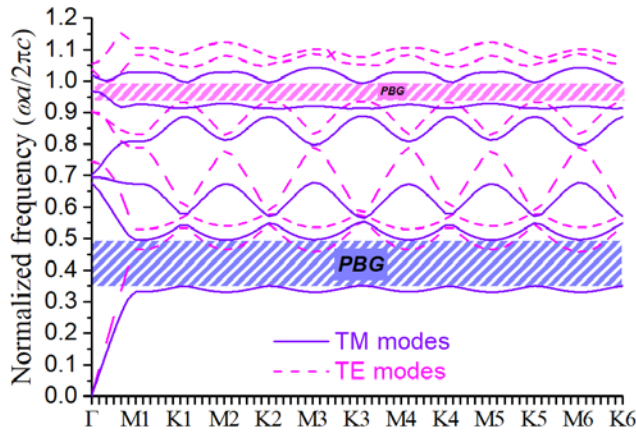


FIGURE 22. Band diagram of the PhC corresponding to the TE_{12} modes optimized for maximum PBG (TM modes are represented in solid lines and TE modes in dashed ones). The correspondence between the x-axis and the key points at the edges/corners of the first Brillouin zone is found in Fig 2.

C. RE-SCALING THE OPTIMIZED SIC STRUCTURE TO BUILD BLOCKS OF COMPONENT FOR OPERATION AT $\lambda = 1.5 \mu m$

Since then, our work in this project assumed the inverse design of PhCs with a band diagram normalized to the lattice constant or periodicity, a , of the crystal. In order to make our final designs realizable, the next step is to rescale the optimized unit cell to an operating wavelength of a given application since the Maxwell equations are scalable. Thus, we choose the normalized central frequency of the PBG shown in Fig 22, i.e., $\omega a / (2\pi c) = 0.4218$, and after using the following relation $a/\lambda = 0.4218$ to rescale the optimized structure to $\lambda = 1.5 \mu m$, we obtained the lattice constant $a \sim 0.633 \mu m$.

Once we have the final geometry sizes, wavelength, and material properties, we used a commercial electromagnetic solver also based on FEM, COMSOL Multiphysics [33], to simulate the response of the optimized PhCs, for TM polarization, but now, assuming a certain periodicity, instead of just the unitary cell.

Figure 23 shows the spectral response of transmitted light through the optimized structure under the normal incidence of TM-polarized light, assuming structures comprised of six periods, as shown in the inset.

As described in equation 1, TE modes have a component of the electric field in the z-direction. We are showing in the inset the amplitude of this component, and it can be observed that the electric field cannot propagate inside the structure as one sees in Fig. 23, when the optimized unit cells are arranged to comprise structures of only 6 periods, its reflectance assumes values as high as 100% when the incident light has wavelengths inside the PBG. As described in equation 1, TM modes have a component of the electric field in the z-direction. We are showing in the inset the amplitude of this component, and it can be observed that the electric field cannot propagate inside the structure; in this

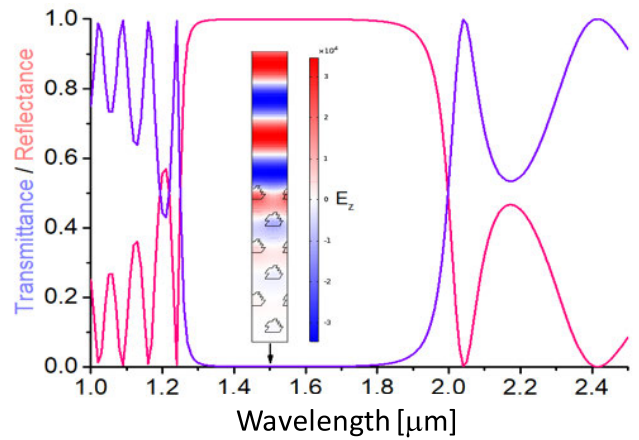


FIGURE 23. Transmittance and reflectance versus wavelength for TM polarization. The inset shows the z-component of the electric field at $\lambda = 1.5 \mu m$ under the normal incidence of a plane wave to the PhC interface.

way, the inset from this figure shows the distribution of the E_z component of the TM light inside and outside the PhC, at $\lambda = 1.5 \mu m$; highlighting the complete reflection of light in the PBG region. Additionally, it is also noticed that almost the total field is entirely reflected at the 5th PhC period; such behavior also occurs in PhCs with regular geometries.

IV. CONCLUSION

We introduced a model based on an artificial immune system algorithm developed to solve the inverse design of photonic bandgap materials. Its results are compared with the results of the Artificial Bee Colony algorithm and Genetic algorithm applied to the same type of problem.

The model was presented and assessed by the inverse design of large photonic bandgaps in two-dimensional photonic crystals. Large photonic bandgaps were obtained in PhCs, comprised of silicon and air, for TE and TM polarizations, and those results were compared to the literature. Additionally, a new PhC design based on SiC and air, with an optimized PBG of 33.94% for the TM polarization, was obtained by this model.

Although it may be impracticable to map the entire search space, especially if the search space gets more refined, In addition, from the obtained results, we can affirm that the algorithm dynamically adjusts the population size, exploration, and exploitation of the search space; location of multiple optima; exhibiting a capability of maintaining many optima solutions as its continuous counterpart presented in [20]. Moreover, good population stabilization was also noticed for long intervals of generations, managed by the network suppression threshold defined by the photonic crystal filling fraction. The proposed model showed fast fitness convergences; at the time, it did not harm the quality of the results when comparing these with results reported in the literature. Interestingly, the intrinsic characteristics of this model, inspired by AIS, allow the designer to get

insights regarding the solution to the problem. As an example, we mention Fig. 10 and Fig. 19 showing the relation of the fitness versus filling fraction of the memory cells, where one can note the highest fitness occurs around specific ranges of filling fraction. Thus, the model can also be used to start an inverse design in a coarse mesh/domain and start a subsequent optimization in a fine mesh/domain in a search space nearby that one with higher fitness versus filling fraction. However, this subsequent optimization must not necessarily be carried out by the opt-aiNET algorithm; it could be performed by one more suitable for local search. Another improvement suggestion regards the population size. As one of the main features of that algorithm is the dynamic population size, it may be interesting to assume, in future works, some mechanism for managing the maximum number of memory cells while maintaining the population size variable. Finally, we demonstrated that the present proposal is a useful approach for the inverse design of PhC, and we believe it is also interesting to the inverse design problems, in general, when the search space is discretized in a binary-valued domain.

CREDIT AUTHORSHIP CONTRIBUTION STATEMENT

Gilliard N. Malheiros-Silveira: Conceptualization, Formal analysis, Data curation, Investigation, Methodology, Software, Visualization, Validation, Writing – original draft, Writing – review & editing. Vitaly F. Rodríguez-Esquerre: Conceptualization, Software, Resources, Writing – review.

DECLARATION OF COMPETING INTEREST

The authors declare that they have no known competing financial interests or personal relationships that could have appeared to influence the work reported in this paper.

DATA AVAILABILITY

Data will be made available on request.

REFERENCES

- [1] E. Yablonovitch, "Inhibited spontaneous emission in solid-state physics and electronics," *Phys. Rev. Lett.*, vol. 58, no. 20, pp. 2059–2062, May 1987.
- [2] J. D. Joannopoulos, S. G. Johnson, J. N. Winn, and R. D. Meade, *Photonic Crystals: Molding the Flow of Light*. Princeton, NJ, USA: Princeton Univ. Press, 2008.
- [3] M. Rachana, S. Swarnakar, M. R. Babu, P. M. Swetha, Y. P. Rangaiah, S. V. Krishna, and S. Kumar, "Optimization of an all-optical three-input universal logic gate with an enhanced contrast ratio by exploiting a T-shaped photonic crystal waveguide," *Appl. Opt.*, vol. 61, pp. 8162–8171, Oct. 2022.
- [4] M. Rachana, S. Swarnakar, N. H. Priya, S. V. Krishna, P. S. Sharma, and S. Kumar, "High-speed optimisation of an all-optical half adder using a T-shaped photonic crystal waveguide with an improved contrast ratio," *Pramana*, vol. 96, no. 4, p. 174, Sep. 2022.
- [5] G. N. Malheiros-Silveira and H. E. Hernandez-Figueroa, "Prediction of dispersion relation and PBGs in 2-D PCs by using artificial neural networks," *IEEE Photon. Technol. Lett.*, vol. 24, no. 20, pp. 1799–1801, Oct. 2012.
- [6] A. S. Ferreira, G. N. Malheiros, and H. E. Hernández, "Computing optical properties of photonic crystals by using multilayer perceptron and extreme learning machine," *J. Lightw. Technol.*, vol. 36, no. 18, pp. 4066–4073, Sep. 15, 2018.
- [7] T. Asano and S. Noda, "Optimization of photonic crystal nanocavities based on deep learning," *Opt. Exp.*, vol. 26, no. 25, pp. 32704–32717, 2018.
- [8] R. Abe, T. Takeda, R. Shiratori, S. Shirakawa, S. Saito, and T. Baba, "Optimization of an H0 photonic crystal nanocavity using machine learning," *Opt. Lett.*, vol. 45, no. 2, pp. 319–322, 2020.
- [9] P. R. Wiecha, A. Y. Petrov, P. Genevet, and A. Bogdanov, "Inverse design of nanophotonic devices and materials," *Photon. Nanostruct.-Fundam. Appl.*, vol. 52, Oct. 2022, Art. no. 101084.
- [10] Y. Zheng and Z. Wu, *Intelligent Nanotechnology, Merging Nanoscience and Artificial Intelligence, Materials Today*. Amsterdam, The Netherlands: Elsevier, 2023.
- [11] G. N. Malheiros-Silveira and F. G. Delalibera, "Inverse design of photonic structures using an artificial bee colony algorithm," *Appl. Opt.*, vol. 59, pp. 4171–4175, May 2020.
- [12] R. D. Meade, A. M. Rappe, K. D. Brommer, J. D. Joannopoulos, and O. L. Alerhand, "Accurate theoretical analysis of photonic band-gap materials," *Phys. Rev. B, Condens. Matter*, vol. 48, no. 11, pp. 8434–8437, Sep. 1993.
- [13] S. Guo, F. Wu, S. Albin, and R. S. Rogowski, "Photonic band gap analysis using finite-difference frequency-domain method," *Opt. Exp.*, vol. 12, pp. 1741–1746, Apr. 2004.
- [14] M. Marrone, V. F. Rodriguez-Esquerre, and H. E. Hernandez-Figueroa, "Novel numerical method for the analysis of 2D photonic crystals: The cell method," *Opt. Exp.*, vol. 10, pp. 1299–1304, Nov. 2002.
- [15] G. N. Malheiros-Silveira, V. F. Rodriguez-Esquerre, and H. E. Hernandez-Figueroa, "Strategy of search and refinement by GA in 2-D photonic crystals with absolute PBG," *IEEE J. Quantum Electron.*, vol. 47, no. 4, pp. 431–438, Apr. 2011.
- [16] G. N. Malheiros-Silveira and V. F. Rodriguez-Esquerre, "Photonic crystal band gap optimization by generic algorithms," in *IEEE MTT-S Int. Microw. Symp. Dig.*, Oct. 2007, pp. 734–737.
- [17] S. Preble, M. Lipson, and H. Lipson, "Two-dimensional photonic crystals designed by evolutionary algorithms," *Appl. Phys. Lett.*, vol. 86, no. 6, Feb. 2005, Art. no. 061111.
- [18] D. Karaboga and B. Basturk, "A powerful and efficient algorithm for numerical function optimization: Artificial bee colony (ABC) algorithm," *J. Glob. Optim.*, vol. 39, no. 3, pp. 459–471, 2007.
- [19] L. N. de Castro and F. J. Von Zuben, "Learning and optimization using the clonal selection principle," *IEEE Trans. Evol. Comput.*, vol. 6, no. 3, pp. 239–251, Jun. 2002.
- [20] L. N. de Castro and J. Timmis, "An artificial immune network for multimodal function optimization," in *Proc. Congr. Evol. Comput.*, 2002, pp. 699–704.
- [21] K. Sakoda, *Optical Properties of Photonic Crystals*. Berlin, Germany: Springer-Verlag, 2005.
- [22] J. Jin, *The Finite-Element Method in Electromagnetics*. New York, NY, USA: Wiley, 1993.
- [23] A. D. Sisnando, L. Vieira, V. F. R. Esquerre, and F. G. S. Silva, "Artificial immune system optimisation of complete bandgap of bidimensional anisotropic photonic crystals," *IET Optoelectron.*, vol. 9, no. 6, pp. 333–340, Dec. 2015.
- [24] C. D. Salzberg and J. J. Villa, "Infrared refractive indexes of silicon, germanium and modified selenium glass," *J. Opt. Soc. Amer.*, vol. 47, no. 3, pp. 244–246, 1957.
- [25] Y.-F. Chau, F.-L. Wu, Z.-H. Jiang, and H.-Y. Li, "Evolution of the complete photonic bandgap of two-dimensional photonic crystal," *Opt. Exp.*, vol. 19, no. 6, pp. 4862–4867, 2011.
- [26] D. Wang, Z. Yu, Y. Liu, P. Lu, L. Han, H. Feng, X. Guo, and H. Ye, "The optimal structure of two dimensional photonic crystals with the large absolute band gap," *Opt. Exp.*, vol. 19, no. 20, pp. 19346–19353, 2011.
- [27] S. Molesky, Z. Lin, A. Y. Piggott, W. L. Jin, J. Vuckovic, and A. W. Rodriguez, "Inverse design in nanophotonics," *Nature Photon.*, vol. 12, no. 11, pp. 659–670, 2018.
- [28] J. L. P. Ruiz, A. A. S. Amad, L. H. Gabrielli, and A. A. Novotny, "Optimization of the electromagnetic scattering problem based on the topological derivative method," *Opt. Exp.*, vol. 27, no. 23, pp. 33586–33605, 2019.
- [29] T. Phan, D. Sell, E. W. Wang, S. Doshay, K. Edee, J. Yang, and J. A. Fan, "High-efficiency, large-area, topology-optimized metasurfaces," *Light Sci. Appl.*, vol. 8, p. 48, May 2018.
- [30] R. Mattoso, L. H. Gabrielli, and A. A. Novotny, "Topology design optimization of nanophotonic devices for energy concentration," *Appl. Math. Model.*, vol. 104, pp. 517–530, Apr. 2022.

- [31] A. Yi, C. Wang, L. Zhou, Y. Zhu, S. Zhang, T. You, J. Zhang, and X. Ou, "Silicon carbide for integrated photonics," *Appl. Phys. Rev.*, vol. 9, Sep. 2022, Art. no. 031302.
- [32] J. Y. Lee, X. Lu, and Q. Lin, "High-Q silicon carbide photonic-crystal cavities," *Appl. Phys. Lett.*, vol. 106, no. 4, 2015, Art. no. 041106.
- [33] *COMSOL Multiphysics*. Stockholm, Sweden. [Online]. Available: www.comsol.com



GILLIARD N. MALHEIROS-SILVEIRA (Senior Member, IEEE) was born in Caetité, Brazil. He received the B.Sc. degree in system analysis from Universidade Estadual da Bahia (UNEB), in 2007, the B.Sc. degree in electrical engineering from Instituto Federal da Bahia (IFBA), in 2008, and the M.Sc. and Ph.D. degrees in electrical engineering from the University of Campinas (UNICAMP), Campinas, São Paulo, Brazil, in 2010 and 2014, respectively.

He was a Postdoctoral Researcher with the CCH Optoelectronics Group, University of California at Berkeley, from 2015 to 2016. From 2017 to 2018, he worked on optical fiber-based devices and integrated photonics with CTI Renato Archer, Campinas, a Research and Development Unit of the Brazilian Ministry of Science, Technology, Innovation, and Communication (MCTIC). He was an Assistant Professor with São Paulo State University (UNESP), Brazil, from 2018 to 2021. He was a Visiting Professor with the Department of Electrical Engineering, Federal University of Bahia (UFBA), Salvador, Brazil, from 2021 to 2022. He joined the School of Electrical and Computer Engineering (FEEC), UNICAMP, in June 2022. He is the author and coauthor of 21 articles in international journals, two book chapters, and 45 papers in international conferences. His current research interests include topics related to integrated photonics, inverse design, antennas, and computational intelligence. He is a member of OPTICA (formerly OSA—Optical Society of America) and SPIE societies. He was a Student Member of the IEEE Photonics Society and Antennas and Propagation Society and OPTICA. He is an Academic Editor on the editorial board of the *International Journal of Optics* (Hindawi) and a Topical Advisory Panel Member of *Photonics* (MDPI).



VITALY F. RODRÍGUEZ-ESQUERRE received the B.S. degree in electronic engineering from Antenor Orrego Private University, Trujillo, Peru, in 1994, and the M.Sc. and Ph.D. degrees in electrical engineering from the University of Campinas, São Paulo, Brazil, in 1998 and 2003, respectively. He was an Adjunct Professor with the Federal Center of Technological Education, Bahia, Salvador, Brazil, from 2006 to 2009. He is currently an Associate Professor with the Department of Electrical Engineering, Federal University of Bahia (UFBA), Brazil. His current research interests include optimization and numerical methods for the analysis of electromagnetic fields in conventional and metamaterial-based integrated optics for applications in telecommunications, sensing, and energy harvesting.

• • •